Sensors & Transducers, Vol. 22, Special Issue, June 2013, pp. 36-43

www.sensorsportal.com

Sensors & Transducers

http://www.sensorsportal.com

Design and Distortion Analysis of Passive Sensor Probes for the Measurements in Electric Fields

[1] Zhan-Long Zhang, [1] Ze-Bing Li, [2] Qin Xin, [1] Ping Hu, [1] Dong-Ping Xiao, [1] Wei He

[1] State Key Laboratory of Power Transmission Equipment & System Security and New Technology Chongqing University, 400044, P. R. China

[2] Université Catholique de Louvain, Department of Applied Mathematics, B-1348, Louvain-la-Neuve, Belgium

Fax: +86-23-65102434

E-mail: zhangzl@cqu.edu.cn, lizebing519@163.com

Received: 15 April 2013 /Accepted: 20 June 2013 /Published: 28 June 2013

Abstract: The sensor probes deployed in the electric fields will cause the distortion in the vicinities, therefore it may significantly affect the accuracy of the measurements in the electric fields. In this paper, we propose a novel approach to separate the electric field distortion due to the spherical sensor probes in a uniform electric field. Moreover, we also investigate the impacts of the spherical sensor probes to the original electric field distortion in terms of the size of sensor probes, the electrode materials, the coupling between the polar electrodes in the design of sensor probes. Our simulation results show that a passive electric field sensor system with the bands from 5 Hz to 200 kHz, and a 20 nF capacitance, combining with our new electric field distortion correction scheme, can surprise meet the requirements of the practical engineering. Moreover, our simulation results also show that the electric field sensor probe system we suggested only has 0.16 % nonlinear errors compared with the corresponding original system measurements. We hope our work will stimulate the future research in the design of the sensor probe systems for monitoring of the electric field. *Copyright © 2013 IFSA.*

Keywords: Electric field distortion, Passive sensor probes, High frequency power system.

1. Introduction

Sensor probe systems have extremely large applications in the electric fields, such as measurements of substation power frequency, transmission lines, the fault diagnosis, and monitoring of the power system [1-4]. The sensor probe system was first introduced into electric fields in the 1980s in which the electric field is measured by the acquisition of values of the signals induced between the metal electrodes in the electric field. The electric field sensor probe system has lots of good characters, e.g., good anti-overload protection, low cost, and easy to be implemented [5]. The sensor probes deployed in the electric fields will cause the distortion in the vicinities, therefore it may significantly affect the accuracy of the measurements in the electric fields. Consequently, we need to take into account the distortion induced by the sensor probes in the design of the sensor probe systems in the electric fields. Moreover, proper distortion correction techniques will be also needed to improve the accuracy of the measurements in the electric fields.

Article number P_SI_376

2. Principles of Sensor Measurements

The sensor probe system designed in this work is mainly made for the high-voltage electric fields and strong electric fields. Due to the less distortion, convenience on calculation of the surface electric field and advantage of less point discharge by the spherical aberration [6], we adopt spherical passive sensor probes in our work, see the Fig. 1(a) for the detailed structure.

Assume the electrode surface area is S and the sensor probes are placed in a uniform electric field. When the induced charges will not change anymore on the spherical sensor probes, a stable distribution of the external electric field at the sensor probes is reached. According to the MAXWELL equation and the electric field theory, the potential distribution of external electric field satisfies the Laplace equation [7], which can be expressed as follows.

$$Q(t) = \iint_A \sigma(t,\theta)ds = \int_0^{\frac{\pi}{2}}\int_0^{\frac{\pi}{2}} \sigma(t,\theta) r^2 \sin\theta d\theta d\varphi = 3\pi r^2 \varepsilon E_0(t) \tag{1}$$

In the actual measurement system, it includes the inherent capacitance of C_k, the measuring capacitance of symmetric electrodes C_m, the entrance to the circuit capacitance probe C_i and R_k of sampling capacitor resistance itself, the entrance resistance measuring circuit R_i and the resistance between the two shells R_c parallel composition. Therefore, the entire sensor probe system is equivalent to the following circuit as shown in Fig. 1(b).

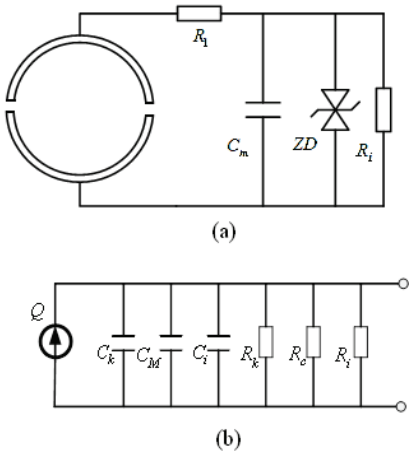

Fig. 1. Schematic diagram of the current transducer and the equivalent circuit of sensor probe system.

According to Kirchhoff's Current Law [8], we know that

$$\frac{dQ_m(t)}{dt} = (C_k + C_m + C_i)\frac{dU_m}{dt} + \frac{U_m(t)}{R_k // R_c // R_i} \tag{2}$$

Since the resistance of the sampling capacitor R_k and the two shells resistor R_c are up to 1000 MΩ, the inherent capacitance of the electrode C_k and the entrance of the probe circuit capacitance C_i are less than 10PF, the Eq. (2) can be rewrote as a vector format as follows.

$$j\omega \vec{Q}_m = j\omega C_m \vec{U}_m + \frac{\vec{U}_m}{R_i} \tag{3}$$

Combining with Eq. (1), the following equation can be obtained.

$$\vec{U}_m = \frac{j\omega 3\pi r^2 \varepsilon \vec{E}_0}{j\omega C_m + 1/R_i} \tag{4}$$

It is easy to see that the measurements in the electric field are heavily depend on the frequency of electric field, the size of the probes, the capacitances of the sensor probes and resistors. In order to optimize the electric field sensor system, t we are focusing on the impact of the size of the sensor probes to the electric field measurements in terms of the distortion.

3. Distortion of the Electric Field

Any conductor in an electric field, electric field will cause the movement of the charge in the conductor surface. Similarly the charge on a conductor also produces an electric field. The induced electric field can superimpose on the original electric field and change the electric field near the conductor. Moreover, the field around the conductor is called as "distortion field." The sensor probes deployed in the electric fields will cause the distortion in the vicinities, therefore it may significantly affect the accuracy of the measurements in the electric fields. Assume that an infinite uniform electric field and the dielectric constant is ε_1 and the dielectric electrode is ε_2 and electric field strength is *E*. The potentials both inside and outside consist of two components due to the deployment of the sensor probes into the electric field.

$$\begin{aligned} U_1 &= U_0 + U_{1a} \\ U_2 &= U_0 + U_{2a} \end{aligned} \tag{5}$$

where U_1 and U_2 are the internal and external potential of spheres respectively, U_0 refers to the

non-uniform electric field measurement sensor potential, U_{1a} and U_{2a} denote the internal and external electric field induced distortion generated by potentials. Therefore, the analysis of electric field distortion mainly refers to solve the distortion potential value U_{1a} and U_{2a}.

When the induced charge distribution in the surface of the spherical sensor probes reaches a stable electric field, the potential distribution of the external electric field satisfies the Laplace equation:

$$\nabla^2 U = 0$$

Assume that Q is an arbitrary point from outside of the space, $\vec{r}$ is a vector from the origin to the point Q, the θ is angle between the axis Z and $\vec{r}$. Consequently, the potential of any point at outside space satisfies the Laplace equation which is:

$$\frac{1}{r^2}\frac{\partial}{\partial r}(r^2\frac{\partial U}{\partial r})+\frac{1}{r^2\sin\theta}\frac{\partial}{\partial\theta}(\sin\theta\frac{\partial U}{\partial\theta})+\frac{1}{r^2\sin^2\theta}\frac{\partial^2 U}{\partial\phi^2}=0 \quad (6)$$

When the induction potential in spherical coordinates satisfies the following conditions: (1) when $r=0$, the potential is $U_2 \to 0$ of the internal spherical; (2) when $r \to \infty$, the potential is $U_1 = -Er\cos\theta$ of the external spherical; (3) when the charge on the spherical sensor probes is continuous distributed, the potentials on the spherical surface are equal which means that

$$\begin{cases} U_1 = U_2 \\ \varepsilon_1 \dfrac{\partial U_1}{\partial r} = \varepsilon_2 \dfrac{\partial U_2}{\partial r} \end{cases} \quad (r = r_0)$$

If the uniform electric field $\vec{E}$ and axis Z of the spherical coordinates follow the exactly same direction, it is well know that U is irrelevant with φ according to the property of symmetry. Eq. (6) can be simplified to:

$$\frac{1}{r^2}\frac{\partial}{\partial r}(r^2\frac{\partial U}{\partial r})+\frac{1}{r^2\sin\theta}\frac{\partial}{\partial\theta}(\sin\theta\frac{\partial U}{\partial\theta})=0 \quad (7)$$

Let $U(r,\theta)=R(r)\Psi(\theta)$, we can obtain that

$$\frac{1}{r^2}\frac{d}{dr}(r^2\Psi\frac{dR}{dr})+\frac{1}{r^2\sin\theta}\frac{d}{d\theta}(R\sin\theta\frac{d\Psi}{d\theta})=0 \quad (8)$$

By dividing by $R(r)\Psi(\theta)$, we can derive the following two equations.

$$\frac{1}{\sin\theta}\frac{d}{d\theta}(\sin\theta\frac{d\Psi}{d\theta})+\mu\Psi=0 \quad (9)$$

$$\frac{d}{dr}(r^2\frac{dR}{dr})-\mu R=0 \quad (10)$$

,

where μ is the constant.

Let $x=\cos\theta, y(x)=\Psi(\theta)$, then Eq. (9) can be reduced to the Legendre equation as follows:

$$\frac{d}{dr}\left[(1-x^2)\frac{dy}{dx}\right]+\mu y=0 \quad -1\le x\le 1 \quad (11)$$

,

where the condition for μ to satisfy the potential is limited in the given area is $\mu=n(n+1), n=1,2,|\cdots$. Under such an assumption, the Eqs. (10) and (11) can be rewritten as:

$$\frac{d}{dr}(r^2\frac{dR}{dr})-n(n+1)R=0 \quad (12)$$

$$\frac{d}{dr}\left[(1-x^2)\frac{dy}{dx}\right]+n(n+1)y=0 \quad (13)$$

The general solutions for the two equations above can be given by

$$\begin{cases} R(r)=Ar^n+B\dfrac{1}{r^{n+1}}\text{（A、B is any number）} \\ y(x)=P_n(x), or\ \Psi(\theta)=P_n(\cos\theta), n=0,1,2\cdots \end{cases} \quad (14)$$

Thus, the particular solution for Eq. (7) in the bounded area is

$$U_n(r,\theta)=(Ar^n+B\frac{1}{r^{n+1}})P_n(\cos\theta), n=0,1,2\cdots \quad (15)$$

The general solution of the potential distribution can be obtained by superposition of all special solutions that satisfies the condition Eq. (15).

$$U(r,\theta)=\sum_{n=0}^{\infty}(A_n r^n+B_n\frac{1}{r^{n+1}})P_n(\cos\theta), n=0,1,2,\cdots \quad (16)$$

,

where and A_n and B_n are the constants that need to be fixed later.

According to the limit boundary conditions in the induced potentials, we can obtain:

$$U_1=-\frac{3\varepsilon_1}{2\varepsilon_1+\varepsilon_2}Er\cos\theta \quad (17)$$

$$U_2=-Er\cos\theta-\frac{\varepsilon_2-\varepsilon_1}{2\varepsilon_1+\varepsilon_2}\frac{r_0^3}{r^2}E\cos\theta \quad (18)$$

where $\frac{\varepsilon_2 - \varepsilon_1}{2\varepsilon_1 + \varepsilon_2}\frac{r_0^3}{r^2}E\cos\theta$ is the distortion caused by the spherical sensor probes in the potential of the external electric field U_2. Consequently, we can know that the electric field distortion depends on the size of the sensor probes, the measure distance and the dielectric coefficients.

3.1. Distortion Analysis due to the Occupied Spaces

The distortion can be different when the spaces occupied by the sensor probes are different. When the sensor probes are located into the monitoring electric field, the spatial distribution of power line change will occur and the power lines around the sensor probes are shifted which result in the distortion of the electric field around the sensor probes. Fig. 2(a) and Fig. 2(b) are distortion distribution in the horizontal and vertical electric field at different distances for the sensor probes with the diameters of 30 mm, 100 mm, 200 mm respectively.

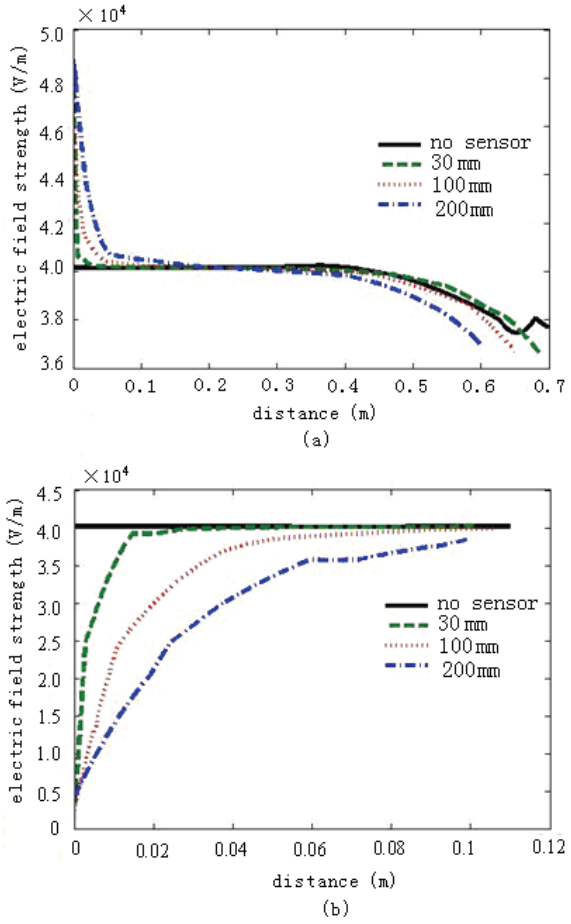

Fig. 2. Transverse electric field and longitudinal electric field distortion at different distances.

We observe that the potentials of the electric field are greater than 46 kV/m at 2 cm in horizontal distance meanwhile the filed strength is only 0.5 kV/m at the vertical direction. The larger size of the sensor probes in the horizontal will cause the larger distortion in the electric field whereas the size of the sensor probes in vertical direction will affect the distortion of the electric field too much.

3.2. Distortion Analysis due to the Materials

Dielectric materials with different coefficients will have the different induced charge and polarization in the electric field which will lead to the different distortion in the electric field. In the electric fields with high voltages, the dielectric polarization will occur that also results in the space charge. The presence of space charge will cause the distortion in the electric field nearby. Consequently, the distribution of the electric field will also be changed, e.g., it may weaken or strengthen the local electric field. Assume that the uniformed dielectric spheres (e.g., spherical sensor probes) are installed in a uniform electric field E_0. It is clear that the dielectric sphere polarization will happen in such an electric field. According to the work in [9-10], the polarization strength can be calculated by

$$P_0 = X_e \varepsilon E_0, \tag{19}$$

where X_e is the proportionality factor and the ε is the dielectric coefficient.

In order to analyze the impacts to the distortion of the electric field generated by the different dielectric coefficients, we investigate the scenario with the copper spherical sensor probe, plastic one and resin one in a uniform electric field. The simulation results are shown in Fig. 3.

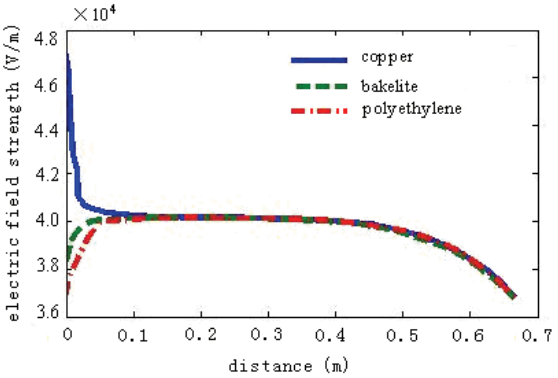

Fig. 3. The distortions by the probes with different materials.

We can easily see the electric field distortion caused by the copper spherical sensor probe is larger

than others because the resistance of copper material is relatively small and the surface of the probe has induced charge. Due to the high impedance for plastic and resin materials, the electric field distortion is relatively small.

3.2. Distortion Analysis due to the Coupling

For a spherical sensor probe, we can establish the corresponding coordination system, e.g., and the electrodes of the sensor probe correspond to the axes. If the incident electric field has only a Z-axis direction electric field, there only exists the electric field in the Z-axis direction of the electrode in the ideal conditions, e.g., no electric field in other two directions. However, in the actual situation, the electric field exists not only on the Z-axis electrode field of the sensor probe but also on the X-axis and Y-axis of the electrode field.

Treat each electrode of the spherical sensor probe as a point. Consequently, the line between two points corresponds to the capacitor. An inter-capacitance can be formed due to the coupling effect between the adjacent electrodes of the sensor probe. An equivalent capacitor network is shown in Fig. 4 (a).

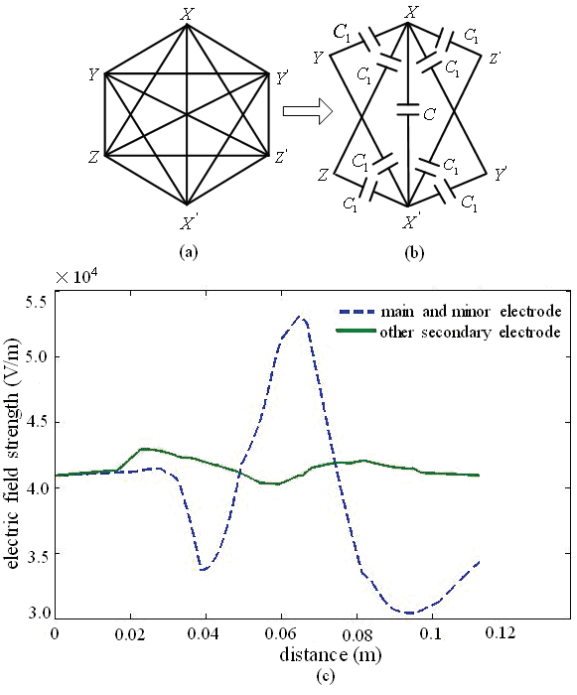

Fig. 4. The equivalent capacitance network model of the probe.

Let $X-X'$ be the main measurement Electrode, then the potentials at Y, Y', Z, Z' will be equal. A simplified capacitance network can be presented as the one shown in Fig. 4 (b). Let the capacitance between the opposite capacitor plates be C and the capacitance between adjacent boards is C_1. When $X-X'$ is the main measurement electrode, the inherently equivalent capacitance of electrode is $C_c = 2C_1 + C$. Therefore, we have

$$U = \frac{Q}{C} + \frac{Q}{2C_1}.$$

Consequently, the measurement of electric potential has been increased by

$$\frac{Q}{2C_1}.$$

The Fig. 4(c) shows the distributions of electric field between the main electrodes and the deputy electrodes and among the deputy electrodes of the sensor probe. Because the critical coupling is between pairs of electrodes among the main electrodes and deputy electrodes, the electric field distortion produced is also large among them. According to the Fig. 4(c), we can see that the distortion rate can be up to 35 %. On the other hand, the distortion caused by the pairs of electrodes among the deputy electrodes of the sensor probe is relatively small.

In the field measurement test, the three-dimensional electrodes of the sensor probe correspond to X, Y, Z axis in the coordinate system. Moreover, the induced voltages U_x, U_y, U_z correspond to E_x, E_y, E_z. In the actual measurement, the value of each element U_x, U_y, U_z contains three components, e.g., one is self-induced voltage in the corresponding direction of the sensor probe, and the other two are from the sensing voltages from other directions. Since the induced voltage measured by the sensor probe is proportional to the external electric field which has a linear relationship between them that can be expressed in matrix format as follows:

$$\lambda * E = U \rightarrow \begin{bmatrix} \lambda_{11} & \lambda_{12} & \lambda_{13} \\ \lambda_{21} & \lambda_{22} & \lambda_{23} \\ \lambda_{31} & \lambda_{32} & \lambda_{33} \end{bmatrix} * \begin{bmatrix} E_x \\ E_y \\ E_z \end{bmatrix} = \begin{bmatrix} U_x \\ U_y \\ U_z \end{bmatrix},$$

where λ is the impact factor matrix, E is the original electric field at the probe, U is a probe of the induced voltage.

4. Correction of Electric Field Distortion

In the devices generated with a uniform electric field, electric field and its directions are uniquely determined. Therefore, the value of electric field in each single direction can be calculated by solving the matrix factors of the measurement effects respectively for the scenario when the corresponding pair of electrodes is the main measurement electrode.

When the applied electric field direction is on the $X-X'$, the relation among the impact factor, the electric field E_x and induced voltage on the X-axis direction can be expressed by

$$\begin{bmatrix} \lambda_{11} & 0 & 0 \\ \lambda_{21} & 0 & 0 \\ \lambda_{31} & 0 & 0 \end{bmatrix} * \begin{bmatrix} E_x \\ 0 \\ 0 \end{bmatrix} = \begin{bmatrix} U_{x1} \\ U_{y1} \\ U_{z1} \end{bmatrix}$$

Similarly, we can get the corresponding matrixes for the scenarios when $Y-Y'$、$Z-Z'$ are the main measurement electrodes respectively.

$$\begin{bmatrix} 0 & \lambda_{12} & 0 \\ 0 & \lambda_{22} & 0 \\ 0 & \lambda_{32} & 0 \end{bmatrix} * \begin{bmatrix} 0 \\ E_y \\ 0 \end{bmatrix} = \begin{bmatrix} U_{x2} \\ U_{y2} \\ U_{z2} \end{bmatrix}$$

$$\begin{bmatrix} 0 & 0 & \lambda_{13} \\ 0 & 0 & \lambda_{23} \\ 0 & 0 & \lambda_{33} \end{bmatrix} * \begin{bmatrix} 0 \\ 0 \\ E_z \end{bmatrix} = \begin{bmatrix} U_{x3} \\ U_{y3} \\ U_{z3} \end{bmatrix}$$

The initial measurement accuracy is not good enough. Therefore, we should take the samples with the large numerical values in order to improve the accuracy. Eventually, the accuracy can be close to the real value. The impact factor matrix for the sensor probe with diameter 30 mm can be calculated by the method mentioned above:

$$\lambda = \begin{bmatrix} 0.0119120 & 0.0082060 & 0.0088160 \\ 0.0088474 & 0.0112730 & 0.0083805 \\ 0.0084332 & 0.0086993 & 0.0119690 \end{bmatrix}$$

Combining the actual measurement of factor matrix under λ and the induced voltage U with relation equation $\lambda * E = U$, the electric field can be derived. Fig. 5 shows the scenario with a sensor probe of diameter 30 mm.

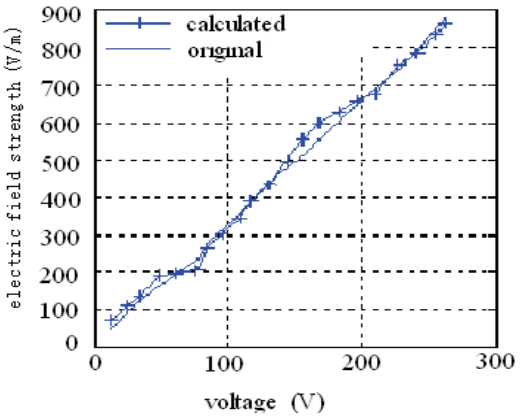

Fig. 5. The results with a 30 mm sensor probe.

It is clear that the resolve solution after distortion in the electric field is very close to the original value. When the probe diameter is 30 mm, the resolved solution of the electric field has the maximum error 13 % and the average error 4.47 %. Therefore, the value of the electric field calculated by this method is much close to the original electric field without the sensor probes. Matrix factors can be seen by the reduction of the probe at the maximum electric field values, help to reduce the impact of distortion on the electric field measurements and improve the accuracy of the measurement field.

5. Experimental Results and Analysis

In order to verify the validity of the electric field sensing system, the parallel plate electrodes in a uniform electric field was calibrated for the test. In accordance with the provisions of the national standard GB/T12720-1991, parallel plate spacing d should be not less than 1.5 times the size of the sensor probe. The sensor probe has at least 2d distance to the bottom edge of the plate electrodes. Moreover, the distance between the parallel plate electrodes to the ground also is set more than 2d [11]. The parallel plate area is 1.5 × 1.5 m, thickness is 2mm and two-plate distance d is 0.5 m. In the experiential test, we employ the copper electrodes with acetylene as the PTFE dielectric. During the tests, the sensor probe is placed in the middle of the parallel plates. Moreover, the direction of electric field induced is perpendicular to the surface of the parallel plates. We also assign the correction factor matrix λ in the sensor signal processing circuit. In order to test frequency response characteristics of the sensor probe system, the sine wave signal and the square signal are investigated. Fig. 6 (a) shows the induced voltage waveforms for corresponding signals by the sensing probe.

We also investigate the impact of the capacitance to the sampling signals. Firstly, we obtain the standard value of the electromagnetic fields at selected points by Italy PMM8035A device. Then the designed sensor system will be in parallel across with the different measurement capacitances. Finally, we chose one suitable capacitance by comparison of the measured electric field strengths with the different capacitances, which has the close performance with the standard values we obtained before. Fig. 6 (b) shows the comparison of the linearity of the data for different CM. We observe that the linearity matches the real data very well when a 20Nf capacitance is adopted. Moreover, the scale factor is between 1.1-1.3.

With the fixed capacitance at 20 nF and the voltage excitation from 0 kV increased to 50 kV, Fig. 7 demonstrates the performance of the sensor probe system we proposed in this work.

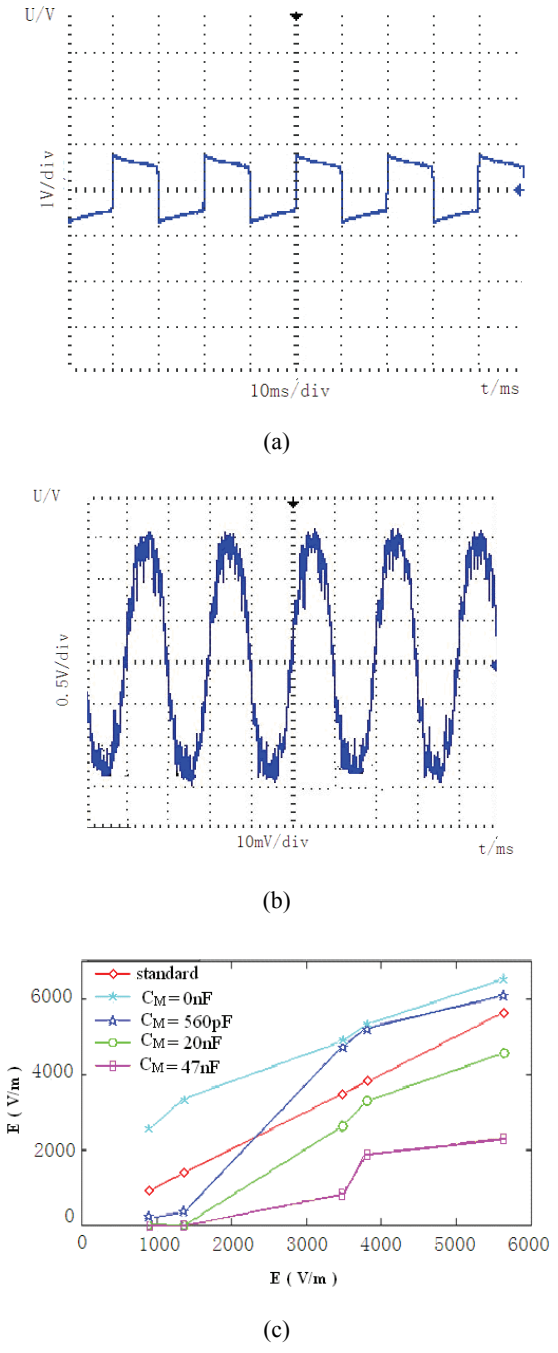

Fig. 6. Induced voltage by the sensor probe and the linearity comparison between different C_M.

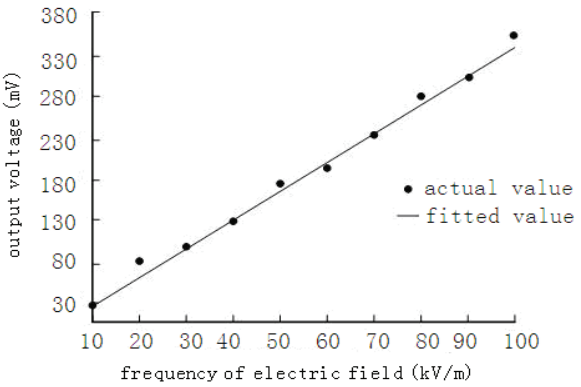

Fig. 7. Experimental result of the Sensing system.

From Fig. 7, we can calculate the fitted function between the output voltage and the electric field intensity, e.g. $U = 3.333E + 3.332$. Consequently, the non-linear error is $e_f = 0.16\%$. It is clear that the external electric field and sensor system output have a good linearity which can perfectly meet the requirements of the practical engineering.

6. Conclusions

In this paper, we propose a novel approach to separate the electric field distortion due to the spherical sensor probes in a uniform electric field. Moreover, we also investigate the impacts of the spherical sensor probes to the original electric field distortion in terms of the size of sensor probes, the electrode materials, the coupling between the polar electrodes in the design of sensor probes. Our simulation results show that a passive electric field sensor system with the bands from 5 Hz to 200 kHz, and a 20 nF capacitance, combining with our new electric field distortion correction scheme, can surprise meet the requirements of the practical engineering. Moreover, our simulation results also show that the electric field sensor probe system we suggested only has 0.16 % nonlinear errors compared with the corresponding original system measurements. We hope our work will stimulate the future research in the design of the sensor probe systems for monitoring of the electric field.

Acknowledgements

This work was supported by The Fundamental Research Funds for the Central Universities (Grant No. CDJZR10150016), and independent research project of the State Key Laboratory of Power Transmission Equipment & System Security and New Technology (Grant No. 2007DA10512712202).

References

[1]. W. Krajewski, Numerical modelling of the electric field in HV substations, *IEE Proc. Science, Measurement and Technology*, Vol. 151, No. 4, 2004, pp. 267-272.

[2]. B. Q. Wan, X. Wu, Y. M. Zhang, S. H. Cao, Y. Zhu, D. S. Shi, Electromagnetic Environment of 750 kV Single-circuit Compact Transmission Lines, *High Voltage Engineering*, Vol. 35, No. 3, 2009, pp. 35, 597-600.

[3]. W. He, F. Yang, J. G. Wang, H. Yang, M. Y. Chen, D. G. Yang, Inverse Application of Charge Simulation Method in Detecting faulty Ceramic Insulators and Processing Influence from Tower, *IEEE Transactions on Magnetics*, Vol. 42, No. 4, 2006, pp. 723-726.

[4]. World Health Organization, Electromagnetic fields and public health: exposure to extremely low

frequency fields, *World Health Organization Fact Sheet*, No 322, Geneva, 2007.
[5]. G. X. Jiang., J. Z. Yang, Power Frequency Electric Field Measurement and the Study of a New Type Measuring Probe, *High Voltage Engineering*, Vol. 1, No. 1, 1985, pp. 1-5.
[6]. Feser K., Pfaff W., A potential free spherical sensor for the measurement of transient electric fields, *IEEE Transactions on PAS*, Vol. 103, No. 10, 1984, pp. 2904. 2911.
[7]. C. R. Li, W. D. Wang, Z. S. Lin, A study of potential-free spherical sensor for transient electric field measurement, *Journal of North China Electric Power University*, Vol. 1, No. 1, 1993, pp. 21-28.
[8]. J. F. Cheng, S. G. Gong, The influence of the electrical field induced by an underwater object, *Journal of Harbin Engineering University*, Vol. 30, No. 7, 2009, pp. 816-819.
[9]. Boggs S., A rational consideration of space charge, *IEEE Electr. Insul. Mag.*, Vol. 20, No. 4, 2004, pp. 22-27.
[10]. Y. X., Zhou B. L. Zhang, D. Bu, N. H. Wang, Y. N Wang, X. D Liang, Z. C Guan, P Yan, Nanosecond pulse corona charging of polymers, *IEEE Trans. on DEI*, Vol. 14, No. 2, 2007, pp. 495-501.
[11]. B. Niu, R. Zeng, H. Li, Design of Non-electrode Power Frequency Electric Field Sensor, in *Proceedings of the CSEE*, Vol. 31, 2008, pp. 101-107.
